

Hysteretic magnetoresistance in superconducting SrTiO₃/LaAlO₃/SrTiO₃ trilayer interface system

Yongsu Kwak^{a,b}, Woojoo Han^{a,c}, Nam-Hee Kim^d, Myung-Ho Bae^{a,c}, Mahn-Soo Choi^e,
Myung-Hwa Jung^f, Yong-Joo Doh^d, Joon Sung Lee^{g,**}, Jonghyun Song^{b,h,*}, Jinhee Kim^{a,***}

^a Korea Research Institute of Standards and Science, Daejeon, 34113, South Korea

^b Department of Physics, Chungnam National University, Daejeon, 34134, South Korea

^c Department of Nanoscience, University of Science and Technology, Daejeon, 34113, South Korea

^d Department of Physics and Photon Science, Gwangju Institute of Science and Technology, Gwangju, 61005, South Korea

^e Department of Physics, Korea University, Seoul, 02841, South Korea

^f Department of Physics, Sogang University, Seoul, 04107, South Korea

^g Display and Semiconductor Physics, Korea University Sejong Campus, Sejong, 30019, South Korea

^h Institute of Quantum Systems (IQS), Chungnam National University, Daejeon, 34134, South Korea

ARTICLE INFO

Keywords:

LaAlO₃/SrTiO₃
SrTiO₃/LaAlO₃/SrTiO₃
Magnetoresistance
Superconductivity
Ferromagnetism
Phase slip center

ABSTRACT

We investigated the electrical transport properties of the SrTiO₃/LaAlO₃/SrTiO₃ (STO/LAO/STO) trilayer interface system. We found that the trilayer exhibits superconductivity at temperatures below 0.2 K. In the superconducting regime, the magnetoresistance (MR) of the system shows pronounced hysteresis, possibly due to the interplay of ferromagnetism and superconductivity. The magnitude of MR hysteresis strongly depends on the magnetic field sweep rate, and we observed a threshold field-sweep rate below which no MR is detected. At high sweep rates, the MR exhibits superconducting-normal-superconducting transition behavior. To explain these observations, we propose a model based on the ohmic heating from superconducting phase slip centers beneath Bloch-type magnetic domain walls in the ferromagnetic layer. Furthermore, we observed complex features in the MR curves that are likely due to domain wall motion in the system.

1. Introduction

The electrical transport properties of oxide heterostructures have garnered significant attention since the discovery of a high-mobility conducting interface between the two band insulators, LaAlO₃ (LAO), and SrTiO₃ (STO) [1]. It is now widely accepted that a conducting two-dimensional electron gas (2DEG) is formed at the interface. Subsequent studies have revealed diverse physical phenomena in the LAO/STO bilayer system, resulting from the correlated interactions between electrons and the lattice. These phenomena include superconductivity [2] and ferromagnetism [3,4].

The formation of a high-mobility 2DEG at the LAO/STO interface can be explained by the polar catastrophe theory [5]. The LAO material consists of two oppositely charged layers, [LaO]⁺ and [AlO₂]⁻, and stacking them creates a buildup of electrical potential. To prevent this

potential from diverging as the thickness increases, half of the electrons at the surface should transfer to the interface. These excess electrons at the interface form a conducting 2DEG. The presence of a critical thickness for electrical conduction supports this explanation. Specifically, the LAO/STO bilayer is non-conducting unless the thickness of the LAO layer is equal to or greater than the critical thickness of 4 unit cells (uc) [6]. However, a recent study by Kwak et al. demonstrated that even a single uc of LAO layer can exhibit nonzero conductivity if the LAO/STO bilayer is covered by another STO capping layer [7].

In this study, we report on the electrical transport properties of an STO/LAO/STO trilayer. The trilayer exhibits superconductivity at temperatures below 0.2 K and displays hysteretic magnetoresistance (MR) behavior upon magnetic field sweep. The MR hysteresis strongly depends on the field sweep rate. When the field sweep rate is smaller than 0.1 mT/s, no MR is observed, and the trilayer remains in the

* Corresponding author. Department of Physics, Chungnam National University, Daejeon, 34134, South Korea.

** Corresponding author.

*** Corresponding author.

E-mail addresses: simmian@korea.ac.kr (J.S. Lee), songjonghyun@cnu.ac.kr (J. Song), jinhee@kriss.re.kr (J. Kim).

<https://doi.org/10.1016/j.cap.2023.06.013>

Received 13 April 2023; Received in revised form 14 June 2023; Accepted 23 June 2023

Available online 27 June 2023

1567-1739/© 2023 Published by Elsevier B.V. on behalf of Korean Physical Society.

superconducting state. However, at a field sweep rate of 0.5 mT/s, the MR curve exhibits a sharp rise and sudden drop in resistance within a certain range of the magnetic field. The peak MR value is close to the normal state resistance of the trilayer, suggesting that superconductivity is completely broken in the resistive region if the field sweep rate is high enough. To explain this characteristic MR behavior, we consider the ohmic heating of phase slip centers (PSCs) in the superconducting layer, which are believed to be generated just above domain walls in the ferromagnetic layer formed at the trilayer interface. The domain wall configuration of the nearby ferromagnetic layer strongly affects the electrical conduction in the superconducting layer. Our proposed model can explain the superconducting-normal-superconducting (S–N–S) transition feature in the MR curve and its dependence on the field sweep rate.

2. Experimental methods

We prepared TiO₂-terminated STO substrates by selectively etching the residual SrO layer using buffered oxide etchant (BOE). The STO substrates were then pre-annealed at a temperature of 950 °C with an oxygen pressure of 2×10^{-5} Torr for 2 h. The LAO and STO films were deposited using the pulsed laser deposition (PLD) method. The STO substrate was maintained at a temperature of 750 °C with an oxygen pressure of 1×10^{-5} Torr. The laser pulse energy was 120 mJ and the repetition rate was 4 Hz. After growth, the samples were annealed in situ in an oxygen-rich atmosphere (500 mTorr) at 750 °C for 30 min and then cooled to room temperature.

For device fabrication, we employed an amorphous-LAO technique. First, we deposited 1 uc of LAO and 1 uc of STO films successively on the STO substrate, as shown in Fig. 1(a) [7]. On the deposited (STO)₁/(-LAO)₁/STO layer, we formed a poly(methyl methacrylate) (PMMA) pattern in the shape of the device conduction path using electron-beam lithography (Fig. 1(b)). Then, we deposited a thick amorphous LAO film at room temperature by PLD. After lift-off, we obtained a pattern as shown in Fig. 1(c). After deposition of an additional 6 uc of STO film, the sample was annealed at a temperature of 750 °C with an oxygen pressure of 1×10^{-5} Torr. Before the STO film deposition, a pre-annealing process was essential to remove PMMA residues and ensure epitaxial growth of STO on top of the (STO)₁/(-LAO)₁/STO film. For electrical

transport measurement, we formed a Ti/Al metal electrode pattern on top of the 2DEG device using electron-beam lithography and sputtering. Fig. 1(e) shows the final form of the fabricated device with the (STO)₇/(-LAO)₁/STO conduction channel. Note that for our sample, electrical transport measurements with the electrical current both parallel and perpendicular to the magnetic field are possible. In this study, we used two such samples named S#1 and S#2.

3. Results and discussions

Fig. 2(a) displays the $R(T)$ curve of sample S#2 in the temperature range of 150 mK–250 mK, with resistance normalized by the value of resistance at $T = 250$ mK (R_n). To obtain this data, we used electrode 1 and 7 in Fig. 1(e) for the current path, and 2 and 3 for the voltage probing. The resistance starts to decrease near 230 mK and reaches zero at 150 mK, with T_c defined as the temperature at which the resistance reaches half of the normal resistance, which is about 170 mK. In Fig. 2(b), we show the I – V characteristics of the sample at a temperature of 20 mK. These characteristics exhibit a significant hysteresis, with widely different superconducting critical current I_c and return current I_r . The large difference between I_c and I_r can be attributed to the Joule heating effect [8]. I_c values in the forward current sweep I_{c+} and the reverse sweep I_{c-} are also different, likely due to the superconducting diode effect [9].

Even after the onset of superconductivity, the resistance decreases slowly with lowering temperature, suggesting the vortex-unbinding transition of a two-dimensional superconductor, known as the Berezinskii-Kosterlitz-Thouless (BKT) transition [10]. As the temperature decreases, the I – V characteristics change from the ohmic behavior $V \propto I$ to the power-law dependence $V \propto I^\alpha$ with $\alpha = 3$ at the BKT transition temperature T_{BKT} . In Fig. 2(c), we illustrate the evolution of I – V characteristics with temperature, while Fig. 2(d) shows α , inferred from the slope of the log-log plot of I – V characteristics, as a function of temperature. Instead of a sharp jump at the BKT transition temperature T_{BKT} , a gradual change of α with temperature is observed near the estimated $T_{\text{BKT}} = 161$ mK. Similar behavior was also observed in LAO/STO bilayers [11].

We conducted measurements of the MR of sample S#2 with a magnetic field applied parallel to the conduction plane. The MR curve of the

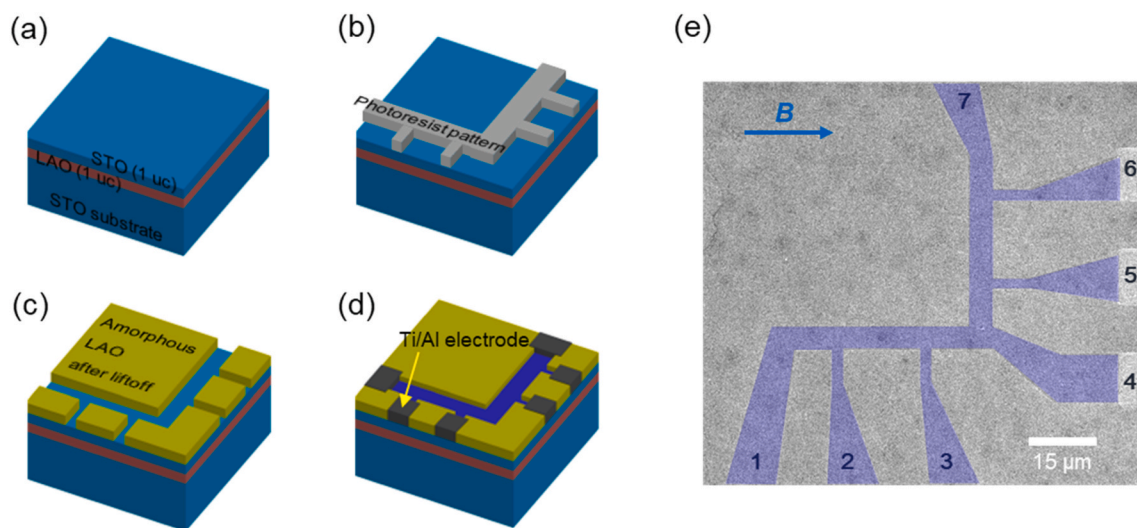


Fig. 1. Sample fabrication scheme. (a) 1 uc of STO and 1 uc of LAO films are deposited on an STO substrate by PLD. (b) An electron-beam lithography process is used to create a PMMA pattern for the conduction path in the device. (c) An amorphous LAO deposition and a lift-off process is used to cover the nonconductive region with an amorphous LAO layer. (d) An additional 6 uc of epitaxial STO is deposited on the device to complete the conduction path, followed by the formation of Ti/Al contact electrodes using electron-beam lithography and sputtering deposition. Note that the STO deposited on the amorphous LAO layer does not make the underlying LAO/STO interface conductive. (e) A scanning electron microscope image of the fabricated device is shown with the conduction channel highlighted in false color. (For interpretation of the references to color in this figure legend, the reader is referred to the Web version of this article.)

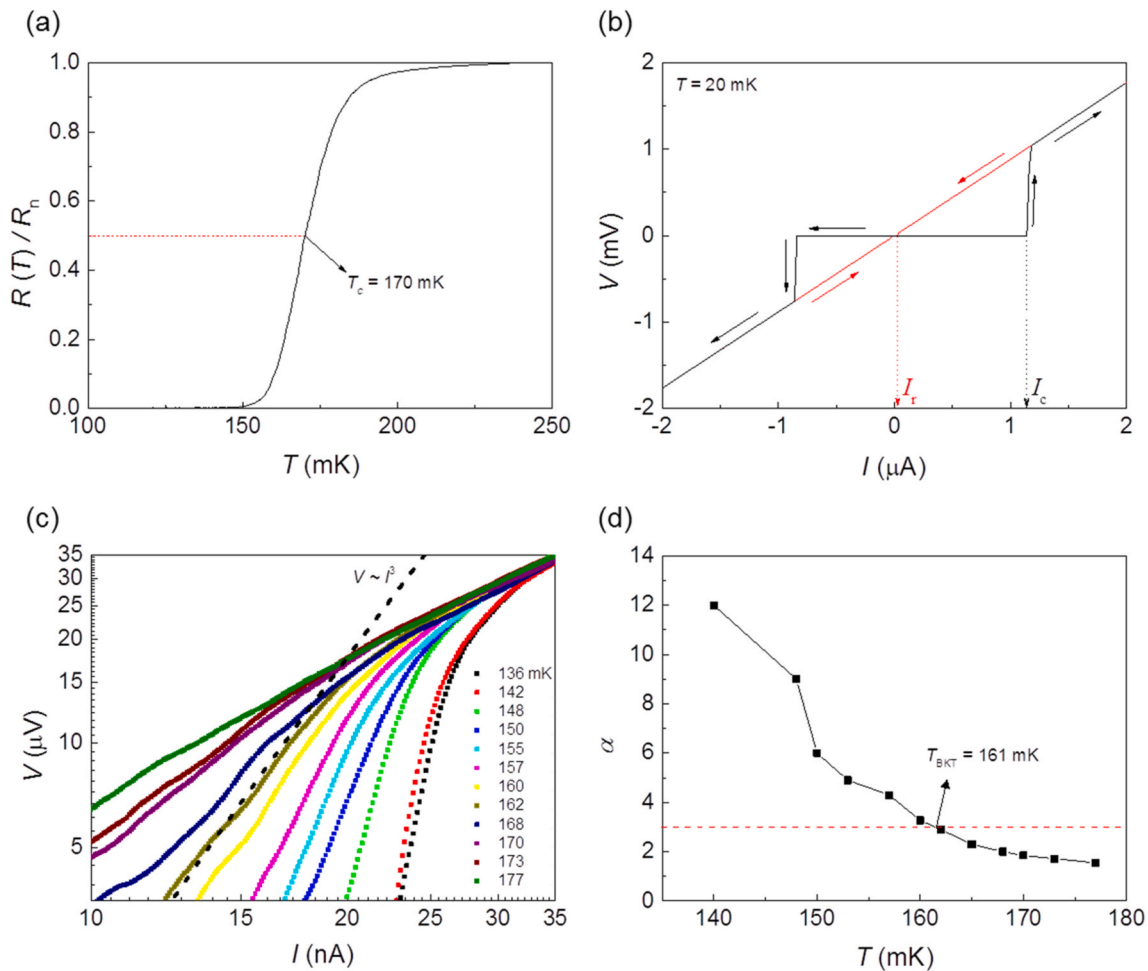


Fig. 2. (a) Temperature dependence of the resistance of sample S#2 measured by the ac 4-probe method. (b) I - V characteristic of the device measured at 20 mK. Superconducting critical currents observed for increasing current bias (critical current I_c) and decreasing current bias (return current I_r) are marked. (c) Evolution of the I - V characteristic with temperature. The device resistance evolves from being ohmic at high temperatures ($T > 177$ mK) to showing an abrupt transition at low temperatures ($T \leq 136$ mK). The curve measured at $T = 162$ mK shows $V \sim I^3$ behavior for lower current bias ($I < 20$ nA). (d) The exponent α obtained from the power-law fitting by $V \propto I^\alpha$ for low bias-current region is shown for the temperatures near the superconducting transition. At the BKT transition temperature T_{BKT} , which is found to be 161 mK, α equals 3.

sample is shown in Fig. 3(a), with a measurement temperature of 20 mK and a magnetic field sweep rate of 0.5 mT/s. We adopted a conventional four probe ac lock-in technique with a bias current of 10 nA. The MR displayed hysteretic behavior depending on the magnetic field sweep direction. Note that the sample was in the superconducting state with zero resistance at both ends of the magnetic field sweep, and a fast field sweep induced a S–N–S transition behavior in the MR curve. The electrical resistance surged up to about 90% of the normal state resistance R_n in the resistive state. The MR hysteresis was insensitive to the relative direction of the current and the magnetic field, as shown in Fig. 3(a) and (b).

We considered several possible explanations for our observations, including giant magnetoresistance (GMR), tunneling magnetoresistance (TMR), and anisotropic magnetoresistance (AMR) effects. However, for the GMR and TMR effects, two ferromagnetic materials with different coercive fields are required. Our sample, however, showed the presence of a single ferromagnetic material (see Supplementary material S1). The MR ratio for the conventional AMR effect is typically less than a few per cent for most ferromagnetic materials, with the exception of unusual giant AMR materials [12]. For our sample, the resistance surged from zero to the normal state resistance, and such a large resistance change cannot be explained by conventional AMR effect.

Fig. 3(c) presents the dependence of the MR curve on the magnetic

field sweep rate. At a sweep rate of 0.1 mT/s, no MR is observed, and the sample remains in the superconducting state during the magnetic field sweep. The in-plane superconducting critical magnetic field of our sample, $H_{c,\parallel}$, is found to be 720 mT at 20 mK (refer to the Supplementary material S2). With a sufficiently slow magnetic field sweep, the superconducting state persists until the magnetic field reaches $H_{c,\parallel}$. The resistive state occurs only if the magnetic field sweep rate is high enough, and the magnetic field is in the range of ± 10 mT to ± 80 mT, which is much smaller than $H_{c,\parallel}$. We suggest that the low magnetic field range may be related to the ferromagnetism of the trilayer. The coexistence of superconductivity and ferromagnetism has already been reported in the LAO/STO bilayer [13,14].

To confirm the ferromagnetism in the trilayer system, we directly measured the magnetic moment. The measured M - H curve exhibits clear hysteresis at a temperature of 1.8 K (refer to the Supplementary material S1). The coercive field was estimated to be 10 mT, and the magnetization was saturated at about 80 mT, implying that the observed resistive state of the MR curve in the magnetic field range of ± 10 mT to ± 80 mT is likely related to the ferromagnetic properties of the trilayer. Although we were unable to measure the M - H curve at temperatures below 1.8 K, it can be assumed that the coercive field of STO/LAO/STO remains almost unchanged in the temperature range where the MR was observed. This assumption is based on the fact that the ferromagnetic

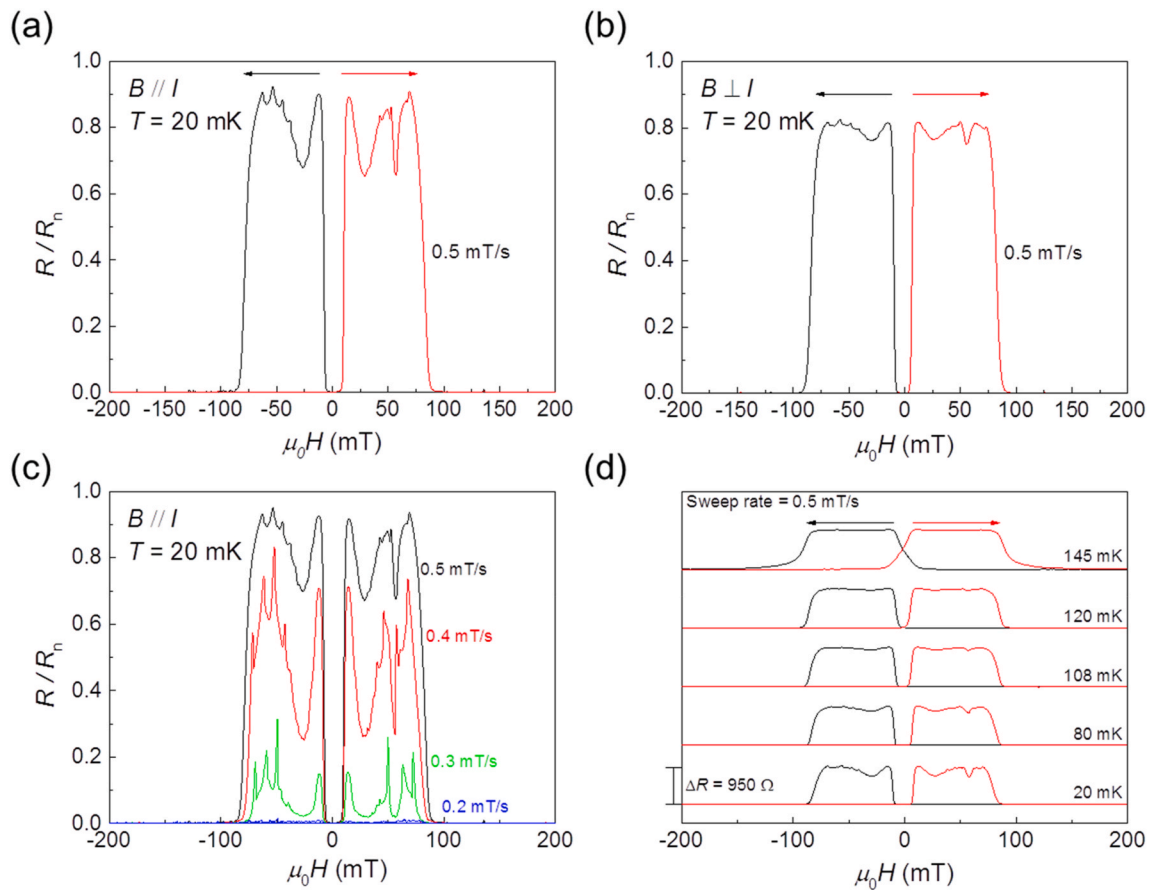


Fig. 3. (a) Normalized magnetoresistance (MR) of device S#2 measured at a temperature of 20 mK, with the magnetic field applied in-plane and parallel to the electric current. The magnetic field sweep rate is set at 0.5 mT/s. (b) Result of a similar MR measurement for the other channel in the same device, with the current is set perpendicular to the applied magnetic field. (c) Evolution of the MR curves with the magnetic field sweep rate. Although the overall shape of the MR curve is maintained, the magnitude of the MR decreases with decreasing sweep rate, and the channel remains superconducting for sweep rates below 0.2 mT/s. (d) The shape of the MR curve changes with the sample temperature. When the sample temperature is set closer to the T_c , the MR curves show wider transition tails, and the $R(T)/R_n$ value is kept closer to unity throughout the magnetic field region of sample magnetization reversal.

dipoles of LAO/STO, measured by Bert et al. using scanning SQUID, do not change in the temperature range from 20 mK to 150 mK [15].

Fig. 3(d) illustrates the temperature dependence of the MR curve, where the magnetic field sweep rate is held constant at 0.5 mT/s. As the temperature increases, the MR curve broadens, and the peak MR value approaches the normal state resistance. The broadening of the MR curve becomes significant as the temperature approaches T_{BKT} . When the magnetic field is swept from -200 mT to $+200$ mT at a sweep rate of 0.5 mT/s, a sharp rise in MR occurs at a magnetic field of $+10$ mT at $T = 20$ mK. However, if the temperature is raised to 145 mK, the MR begins to appear as early as at -20 mT.

The hysteretic MR with the field sweep rate dependence was also observed in an LAO/STO bilayer by Mehta et al. [16]. They explained the hysteretic MR by phase slip across a weak link. In their model, a superconducting layer and a ferromagnetic layer coexist, spatially separated from each other. If a Bloch domain wall exists in the ferromagnetic layer, a magnetic field perpendicular to the layer is allowed, generating magnetic vortices in the superconducting layer. The sweeping magnetic field induces vortex motion, leading to a voltage drop across a weak link. However, Mehta's model is only applicable in the intermediate superconductivity region where the superconductivity is neither too strong nor too weak and cannot explain the S–N–S transition behavior shown in Fig. 3(a).

To explain our experimental results, we consider the thermal heating of a PSC [17]. Similar to the LAO/STO bilayer, we can consider the STO/LAO/STO trilayer as consisting of a ferromagnetic layer and a

superconducting layer that are spatially separated, since the ferromagnetism and superconductivity were also observed simultaneously [7]. The superconductivity in the oxide interface may exhibit significant inhomogeneity due to the variation of oxygen deficiency. Recent studies on LAO/STO bilayer have demonstrated highly non-uniform conduction in the superconducting layer [18]. To model our trilayer system, we assume that the superconducting layer consists of multiple superconducting wires connected in parallel [19].

Fig. 4(a) illustrates our model schematics. When a high magnetic field is applied, the electron spins in the ferromagnetic layer become aligned, and the nearby superconducting layer experiences the sum of the applied magnetic field and the field from magnetization of the ferromagnetic layer. If the total magnetic field to the superconductor is not greater than $H_{c,\parallel}$, the superconductivity persists, and the resistance remains at zero. However, when the magnetic field decreases, magnetic domain walls are created in the ferromagnetic layer. In a Bloch domain wall, magnetic flux perpendicular to the layer is allowed, and magnetic vortices are generated in the superconducting layer. The core of a vortex is in the normal state, and the superconductivity near the vortex is weakened. Thus, a superconducting weak link in the vicinity of a magnetic domain wall can be considered a PSC. By applying external bias current, the PSC can act as a heat source. However, since the typical applied bias current is quite low in general, the heating power of a PSC is too small to significantly increase the temperature of typical low-temperature superconducting device samples. But, if the sample material has sufficiently low heat capacity and thermal conductivity, as STO

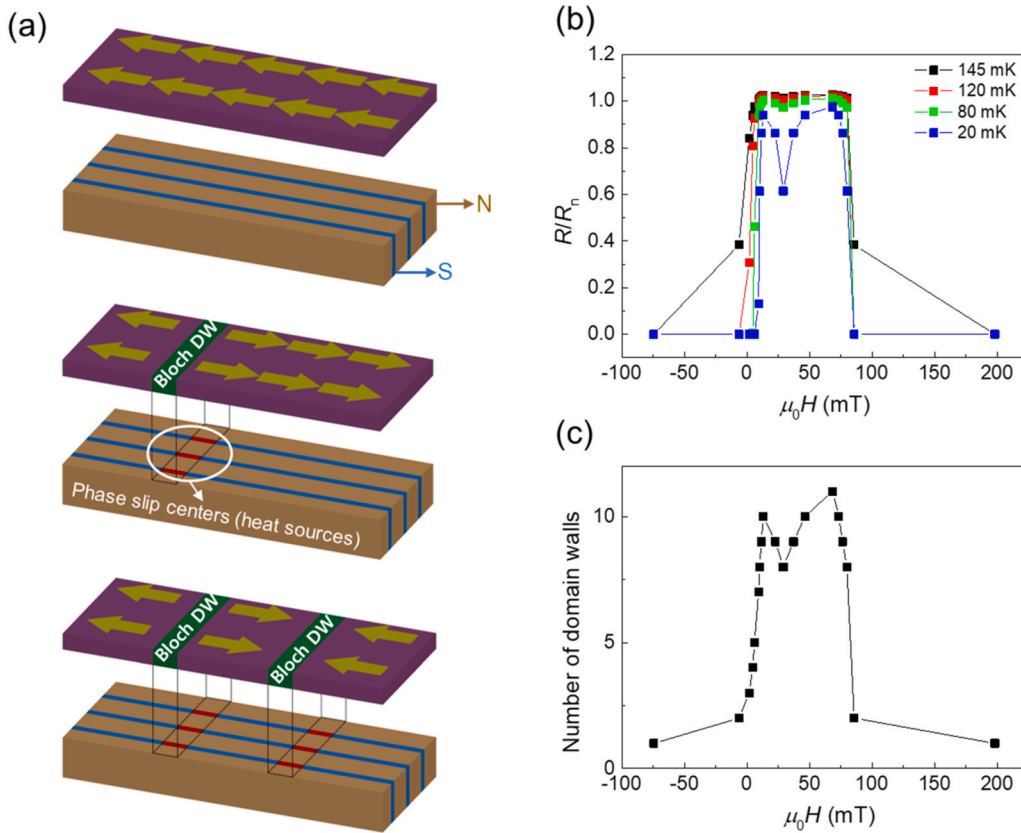


Fig. 4. (a) Schematic of the phase slip center model, where the magnetization in the ferromagnetic (FM) layer is represented as arrows, and the superconducting layer is simplified as a 2D junction array with superconducting pathways, where phase slip centers can form at FM domain boundaries. (b) Results of the thermal simulation described in the main text, showing the temperature dependence of the simulated MR curves, which closely resemble the experimental results presented in Fig. 3(d). (c) The number of the Bloch domains used in the simulation.

does, even a small heating power generated by a PSC can increase the local temperature above the superconducting critical temperature.

Within the framework of the PSC model, our experimental results in Fig. 3(a) can be explained as follows: for a high enough magnetic field, the magnetic moments in the ferromagnetic layer are aligned and no magnetic domain wall exists. The nearby conduction layer remains in the superconducting state unless the applied magnetic field is greater than $H_{c\parallel}$. As the magnetic field decreases, magnetic domain walls are generated in the ferromagnetic layer, and PSCs are formed in the superconducting layer. When combined with the external bias current, heat is generated by the PSCs, raising the local temperature above the superconducting critical temperature and turning the conducting channel into a resistive state. The total resistance increases with the number of PSCs, which should be proportional to the number of magnetic domain walls in the ferromagnetic layer. It is known that the magnetic domain wall density depends on the magnetic field sweep rate; the faster the field sweep rate, the more domain walls are generated [20]. This explains the field sweep rate dependence of our MR curve. Further change of the magnetic field makes the magnetic moments in the ferromagnetic layer aligned in the opposite direction, eliminating domain walls and restoring the superconductivity, completing the S–N–S transition with the magnetic field sweep.

Assuming an external bias current of 10 nA and a normal resistance of 1 k Ω , the electrical power is estimated to be 0.1 pW. Is it possible for such a low electrical power to increase the local temperature from 20 mK (superconducting state) to 200 mK (normal state)? In general, the answer would be ‘No.’ However, in the oxide interface system, an S–N transition is probable even with such a low heat generation. The key factors are the temperature dependences of the specific heat and thermal conductivity of STO, which are known to be very low and show strong temperature dependence ($\sim T^3$) at low temperatures [21]. With such low specific heat, it is easy to increase the local temperature even with a tiny heating power. Additionally, the low thermal conductivity should

hinder heat transfer from the heat source, resulting in a higher temperature in its vicinity.

Based on our model, we have performed a numerical simulation. Fig. 4(b) shows the calculated MR curve for several bath temperatures (See the Supplementary material S3 for the details). Here the normal resistance ratio R/R_n corresponds to the ratio of the normal region in the channel. In the normal region, the local temperature is higher than the superconducting critical temperature. The number of Bloch domain walls is assumed to vary as shown in Fig. 4(c). As depicted in Fig. 4(b), the numerical simulation data fit relatively well with the experimental data. At 20 mK, the peak value of R/R_n is not 1, implying that a certain portion of the channel remains in the superconducting state during the magnetic field sweep. At 145 mK, on the other hand, the peak value of R/R_n is close to 1, suggesting that most of the channel is in the resistive state. The onset field of the resistive state also varies with temperature, as observed in the experiment (Fig. 3(d)).

In the temperature range below 200 mK, any slight change in the ferromagnetic properties of LAO/STO can be disregarded. However, due to the lack of detailed knowledge on the magnetic properties of the trilayer in this temperature range, it is unclear how the magnetic domain wall changes with the magnetic field sweep. The number of domains in Fig. 4(c) is assumed arbitrarily for the sample to reproduce the MR curve shape shown in Fig. 3(a). Nevertheless, the model effectively simulates the evolution of MR curves with increasing temperature without additional arbitrariness.

Several points are noteworthy. First, complex features stand out in the MR for intermediate magnetic field sweep rates. At the field sweep rate of 0.4 mT/s, many peaks are observed in the MR curve, as shown in Fig. 3(c). Although we have no plausible explanation yet, we speculate that each peak could be related to the domain wall motion of the system. In our model calculation, we have assumed that both PSCs and domain walls are stationary during the magnetic field sweep. The sharp peaks, however, imply that the domain wall motion may not be neglected. If

the peaks in the MR curve are related to the domain wall motion, our system can be used as a framework to study the domain wall dynamics: the motion of a magnetic domain wall is measured by the change in resistance in the nearby superconductor. Considering that the superconductor and the ferromagnet are separated by a fraction of a nanometer and a superconductor is a highly sensitive magnetic field detector, we would say that our system may provide one of the most sensitive detection frameworks of the magnetic domain wall motion. Further studies are needed.

4. Conclusion

In summary, we observed a hysteretic magnetoresistance in a superconducting STO/LAO/STO trilayer. The MR hysteresis strongly depends on the magnetic field sweep rate. The observed MR can be explained by the ohmic heating of the phase slip centers in the superconducting layer, which are induced by the magnetic flux threading a magnetic domain wall in the nearby ferromagnetic layer. The specific heat and thermal conductivity of STO become very low at low temperatures, making the system highly susceptible to the heating caused by the phase slip. Additionally, we observed complex fine peaks in the MR, which are presumed to be the result of domain wall motions. Further studies are needed to investigate these peaks and their relationship to the domain wall dynamics in the system.

Credit authorship contribution statement

Yongsu Kwak, Woojoo Han: Methodology, Formal analysis. **Nam-Hee Kim:** Methodology, **Myung-Ho Bae, Mahn-Soo Choi:** Conceptualization. **Myung-Hwa Jung:** Conceptualization, Supervision. **Yong-Joo Doh:** Conceptualization, Supervision. **Joon Sung Lee:** Conceptualization, Supervision. **Jonghyun Song:** Supervision, **Jinhee Kim:** Resources, Supervision.

Declaration of competing interest

The authors declare that they have no known competing financial interests or personal relationships that could have appeared to influence the work reported in this paper.

Acknowledgements

This work was supported by Korea Institute for Advancement of Technology (KIAT) grant funded by the Korea Government (MOTIE) (P0008458, HRD Program for Industrial Innovation), Basic Science Research Program through the National Research Foundation of Korea (NRF) funded by the Ministry of Education (NRF-2020R1A6A1A03047771, NRF-2016R1A5A1008184, NRF-2021R1A2C3012612), NRF funded by the Ministry of Science and ICT (No. 2022M3H4A1A04074153, 2020R1A2C1011000, 2018R1A3B1052827, 2020R1A2C3008044), and Electronics and Telecommunications Research Institute (ETRI) grant funded by the Korean government (22YB1500).

Appendix A. Supplementary data

Supplementary data to this article can be found online at <https://doi.org/10.1016/j.cap.2023.06.013>.

References

- [1] A. Ohtomo, H.Y. Hwang, A high-mobility electron gas at the LaAlO₃/SrTiO₃ heterointerface, *Nature* 427 (2004) 423–426, <https://doi.org/10.1038/nature02308>.
- [2] N. Reyren, S. Thiel, A.D. Caviglia, L.F. Kourkoutis, G. Hammerl, C. Richter, C. W. Schneider, T. Kopp, A.-S. Rüetschi, D. Jaccard, M. Gabay, D.A. Müller, J.-M. Triscone, J. Mannhart, Superconducting interfaces between insulating oxides, *Science* 317 (2007) 1196–1199, <https://doi.org/10.1126/science.1146006>.
- [3] Ariando, X. Wang, G. Baskaran, Z.Q. Liu, J. Huijben, J.B. Yi, A. Annadi, A. R. Barman, A. Rusydi, S. Dhar, Y.P. Feng, J. Ding, H. Hilgenkamp, T. Venkatesan, Electronic phase separation at the LaAlO₃/SrTiO₃ interface, *Nat. Commun.* 2 (2011) 188, <https://doi.org/10.1038/ncomms1192>.
- [4] T.D.N. Ngo, J. Chang, K. Lee, S. Han, J.S. Lee, Y.H. Kim, M. Jung, Y. Doh, M. Choi, J. Song, J. Kim, Polarity-tunable magnetic tunnel junctions based on ferromagnetism at oxide heterointerfaces, *Nat. Commun.* 6 (2015) 8035, <https://doi.org/10.1038/ncomms9035>.
- [5] N. Nakagawa, H.Y. Hwang, D.A. Müller, Why some interfaces cannot be sharp, *Nat. Mater.* 5 (2006) 204–209, <https://doi.org/10.1038/nmat1569>.
- [6] S. Thiel, G. Hammerl, A. Schmehl, C.W. Schneider, J. Mannhart, Tunable quasi-two-dimensional electron gases in oxide heterostructures, *Science* 313 (2006) 1942–1945, <https://doi.org/10.1126/science.1131091>.
- [7] Y. Kwak, W. Han, T.D.N. Ngo, D. Odkhuu, Y.H. Kim, S.H. Rhim, M.-S. Choi, Y.-J. Doh, J.S. Lee, J. Song, J. Kim, Non-BCS-type superconductivity and critical thickness of SrTiO₃/LaAlO₃/SrTiO₃ trilayer interface system, *Appl. Surf. Sci.* 565 (2021), 150495, <https://doi.org/10.1016/j.apsusc.2021.150495>.
- [8] H. Courtois, M. Meschke, J.T. Peltonen, J.P. Pekola, Origin of hysteresis in a proximity Josephson junction, *Phys. Rev. Lett.* 101 (2008), 067002, <https://doi.org/10.1103/PhysRevLett.101.067002>.
- [9] J.-X. Lin, P. Siriviboon, H.D. Scammell, S. Liu, D. Rhodes, K. Watanabe, T. Taniguchi, J. Hone, M.S. Scheurer, J.I.A. Li, Zero-field superconducting diode effect in small-twist-angle trilayer graphene, *Nat. Phys.* 18 (2022) 1221–1227, <https://doi.org/10.1038/s41567-022-01700-1>.
- [10] J.M. Kosterlitz, D.J. Thouless, Ordering, metastability and phase transitions in two-dimensional systems, *J. Phys. C Solid State Phys.* 6 (1973) 1181–1203, <https://doi.org/10.1088/0022-3719/6/7/010>.
- [11] A.M.R.V.L. Monteiro, D.J. Groenendijk, I. Groen, J. de Bruijckere, R. Gaudenzi, H. S.J. van der Zant, A.D. Caviglia, Two-dimensional superconductivity at the (111) LaAlO₃/SrTiO₃ interface, *Phys. Rev. B* 96 (2017), 020504, <https://doi.org/10.1103/PhysRevB.96.020504>.
- [12] R.-W. Li, H. Wang, X. Wang, X.Z. Yu, Y. Matsui, Z.-H. Cheng, B.-G. Shen, E. W. Plummer, J. Zhang, Anomalously large anisotropic magnetoresistance in a perovskite manganite, *Proc. Natl. Acad. Sci. USA* 106 (2009) 14224–14229, <https://doi.org/10.1073/pnas.0907618106>.
- [13] L. Li, C. Richter, J. Mannhart, R.C. Ashoori, Coexistence of magnetic order and two-dimensional superconductivity at LaAlO₃/SrTiO₃ interfaces, *Nat. Phys.* 7 (2011) 762–766, <https://doi.org/10.1038/nphys2080>.
- [14] D.A. Dikin, M. Mehta, C.W. Bark, C.M. Folkman, C.B. Eom, V. Chandrasekhar, Coexistence of superconductivity and ferromagnetism in two dimensions, *Phys. Rev. Lett.* 107 (2011), 056802, <https://doi.org/10.1103/PhysRevLett.107.056802>.
- [15] J.A. Bert, B. Kalisky, C. Bell, M. Kim, Y. Hikita, H.Y. Hwang, K.A. Moler, Direct imaging of the coexistence of ferromagnetism and superconductivity at the LaAlO₃/SrTiO₃ interface, *Nat. Phys.* 7 (2011) 767–771, <https://doi.org/10.1038/nphys2079>.
- [16] M.M. Mehta, D.A. Dikin, C.W. Bark, S. Ryu, C.M. Folkman, C.B. Eom, V. Chandrasekhar, Evidence for charge–vortex duality at the LaAlO₃/SrTiO₃ interface, *Nat. Commun.* 3 (2012) 955, <https://doi.org/10.1038/ncomms1959>.
- [17] M. Sahu, M.-H. Bae, A. Rogachev, D. Pekker, T.-C. Wei, N. Shah, P.M. Goldbart, A. Bezryadin, Individual topological tunnelling events of a quantum field probed through their macroscopic consequences, *Nat. Phys.* 5 (2009) 503–508, <https://doi.org/10.1038/nphys1276>.
- [18] M. Honig, J.A. Sulpizio, J. Drori, A. Joshua, E. Zeldov, S. Ilani, Local electrostatic imaging of striped domain order in LaAlO₃/SrTiO₃, *Nat. Mater.* 12 (2013) 1112–1118, <https://doi.org/10.1038/nmat3810>.
- [19] H. Noad, P. Wittlich, J. Mannhart, K.A. Moler, Modulation of superconducting transition temperature in LaAlO₃/SrTiO₃ by SrTiO₃ structural domains, *J. Supercond. Nov. Magnetism* 32 (2019) 821–825, <https://doi.org/10.1007/s10948-018-4730-8>.
- [20] K. Kudo, K. Nakamura, Field sweep-rate dependence of magnetic domain patterns: numerical simulations for a simple Ising-like model, *Phys. Rev. B* 76 (2007), 054111, <https://doi.org/10.1103/PhysRevB.76.054111>.
- [21] V. Martelli, J.L. Jiménez, M. Continentino, E. Baggio-Saitovitch, K. Behnia, Thermal transport and phonon hydrodynamics in strontium titanate, *Phys. Rev. Lett.* 120 (2018), 125901, <https://doi.org/10.1103/PhysRevLett.120.125901>.